IEEE Access
Multidisciplinary | Rapid Review | Open Access Journal

Received August 22, 2021, accepted September 11, 2021, date of publication September 15, 2021, date of current version October 1, 2021.

Digital Object Identifier 10.1109/ACCESS.2021.3113161

Optimization of Operation Parameters in a Cesium Atomic Fountain Clock Using Monte Carlo Method

HUI LI, YUANBO DU, XIAN YANG, YUNYI GUO, MINGMING LIU, WENBING LI, HONGLI LIU, AND ZEHUANG LU

MOE Key Laboratory of Fundamental Physical Quantities Measurement, Hubei Key Laboratory of Gravitation and Quantum Physics, PGMF and School of Physics, Huazhong University of Science and Technology, Wuhan 430074, China.

Corresponding author: Hongli Liu (liuhongli@hust.edu.cn)

This work was supported in part by the National Natural Science Foundation of China under Grant 11804108, Grant 11774108, and Grant 11904113; in part by the National Key Research and Development Program of China under Grant 2017YFA0304400; and in part by the China Postdoctoral Science Foundation under Grant 2017M612431.

ABSTRACT Number of detected atoms and contrast of Ramsey fringe are critical operation parameters in an atomic fountain clock. To optimize these operation parameters, a Monte Carlo method is utilized to simulate the evolution of the atomic cloud. It is found that the physical variables, including atomic temperature, launching direction of the atomic cloud, and the initial position of the atomic cloud, have a large influence on the ratio of the returning atoms to the launching atoms, and consequently the detected atomic number, and the atomic temperature affects the pattern of the Ramsey fringe. In the experiment, these relevant physical variables are optimized and a returning ratio as high as 8.6%±0.4% is obtained for a cesium atomic fountain with a launch height of 1 m. In addition, the Ramsey fringe is experimentally optimized and the contrast of the central Ramsey fringe reaches 90%. The Monte Carlo method we used is also applicable in similar cold atoms experiments.

INDEX TERMS Cesium atomic fountain clock, Monte Carlo simulation, ratio of the returning atoms, launching direction of atomic cloud.

I. INTRODUCTION

Atomic fountain clocks have various applications in atomic time-keeping [1], [2], tests of general relativity [3], precision measurement physics [4], [5], navigation positioning [6] and geodesy [7]. As the most accurate reproduction of the SI ''second'' definition, atomic fountain clocks have been built in several metrology labs around the world [8]–[10]. Among them, a short-term frequency stability of $1.6 \times 10^{-14}\tau^{-1/2}$ (type-A) is realized at SYRTE-FO2-Cs [11], and a systematic frequency uncertainty (type-B) of 1.1×10^{-16} is evaluated at NIST [12].

The frequency stability of an atomic fountain clock is mainly limited by quantum projection noise and local oscillator noise (Dick effect) [13]. The frequency stability limited by quantum projection noise can be represented as [14]

$$\sigma_{QPN}(\tau) = \frac{1}{\pi Q_a}\sqrt{\frac{T_c}{\tau}}\sqrt{\frac{1}{N_{\text{det}}}}, \tag{1}$$

where T_c is the fountain cycle duration, τ is the measurement time, N_{det} is the number of detected atoms, and $Q_a = \nu_0/\Delta\nu$ is the clock transition quality factor. Here $\Delta\nu$ is the width of the Ramsey fringe, and ν_0 is the clock transition frequency. Thus it is natural to improve the frequency stability by increasing the detected atomic number. The Ramsey fringe contrast is also an important physical parameter that affects the interrogation frequency slope, which also relates to the frequency stability.

In an atomic fountain clock, the detected atomic number can be increased with enhancement of the initial launching atomic number, and the ratio of the returning atoms to the launching atoms (abbreviation for R-L ratio). The initial launching atomic number depends on the parameters of magnetic field and lasers in sequential operation phases

The associate editor coordinating the review of this manuscript and approving it for publication was Giovanni Angiulli.

of magneto-optical trap (MOT), optical molasses (OM) and moving optical molasses (MOM), respectively. Once these parameters are determined, the initial launching atomic number no longer changes significantly. However, the detected atomic number can also be increased by optimizing the R-L ratio. In this paper, we focus on theoretical simulation and experimental optimization of the R-L ratio, aiming to improve the detected atomic number.

Theoretical calculation of the R-L ratio involves tracking the path of individual atoms during the ascent and descent process. However, the atomic launching direction, the gravity axis, and the central axis of the cut-off waveguide (we define it as the mechanical axis) might not align with each other, while the size of the cut-off waveguide might restrict the free atomic motion. Given the complexity that the analytic calculation is facing, Monte Carlo method is used to simulate the evolution of individual atoms. Although the Monte Carlo method is often introduced as an auxiliary tool in the atomic fountain clocks [15]–[18], there are rarely systematic reports on further analysis of the R-L ratio in the atomic fountain. According to the simulation, it is found that the R-L ratio is dependent on several physical variables, including atomic cloud temperature, launching direction of the atomic cloud, and initial position of the atomic cloud. Following the guidance of this simulated dependency, the R-L ratio is optimized in the experiment, and the relationship between the R-L ratio and launching direction of the atomic cloud is verified. By fine adjustment of the C-field amplitude, the contrast of the Ramsey fringe is experimentally optimized as well.

In this paper, we first present our experimental setup in Section 2 so that one can be familiar with the definitions of different axes. The Monte Carlo simulation model is introduced in Section 3, and the experimental results is presented in Section 4, showing good agreements between simulation and experiment. Finally, the conclusion is given in Section 5.

II. EXPERIMENTAL SETUP

A cesium atomic fountain clock is under development at Huazhong University of Science and Technology (HUST) to provide a local time-frequency standard for the construction of the Precise Gravity Measurement Facility (PGMF) [19], and measure the absolute clock transition frequency of Al^+ ion optical clock that is under development in our lab. The physics package of the cesium atomic fountain clock is illustrated in Fig. 1. Relevant components in the physics package include an atomic trapping region, a detection region, and an integrated microwave cavity composed of a state selection cavity and a Ramsey cavity. Below the atomic trapping region, there is a goniometric adjustment unit, allowing a minor tuning of the atomic launching direction independently [20]. The tilt angle alignment of the atomic trapping region with respect to the mechanical axis could be performed by rotating two pairs of adjustment screws in the goniometric adjustment unit, with an adjustment resolution of 50 μrad and a range of $\pm$2 mrad.

In the experiment, thermal atoms emitting from a cesium dispenser are cooled and trapped in the MOT and the OM, followed by launching in the MOM, and are further cooled to $\sim\mu$K temperature through adiabatic cooling [21]. Initial radius of the atomic cloud observed from a CCD camera is $A_0 \sim 1$ mm. In its parabolic flight process, the atomic cloud goes through the middle of the integrated microwave cavity twice. Since the atomic cloud is expanding all the time, when returning back to the integrated microwave cavity (after a time duration of $\sim$0.8 s from launching), the typical diameter of the atomic cloud becomes as large as 25 mm. Limited by the diameter of the cut-off waveguides ($\phi = 12$ mm) that are built into the upper, middle and lower ends of the integrated microwave cavity (see inset of Fig. 1), close to 90% atoms are obstructed by the cut-off waveguide and fail to reach the detection region, resulting in a significant loss of the detected atom number.

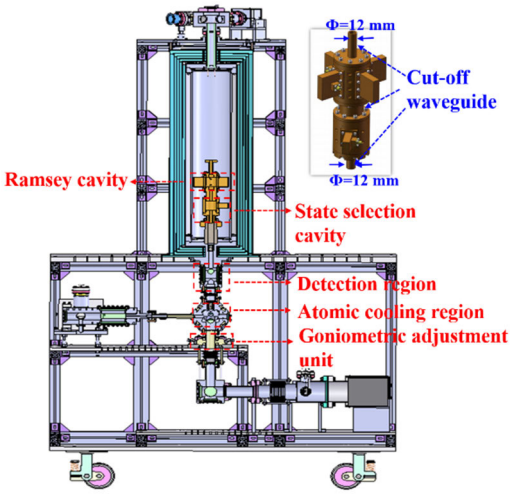

FIGURE 1. Sketch of the cesium atomic fountain physical package. Inset: integrated microwave cavity.

More details about the configuration of the atomic trapping region and the detection region are given in Fig. 2. In the MOT stage, a pair of anti-Helmholtz coils generates a magnetic gradient field near the center of the atomic trapping region, which overlaps with the intersection region of six laser beams with $\sigma^+ - \sigma^-$ polarization, and a beam of repumping laser. The juggling atomic cloud that successfully traverses the cut-off waveguide is probed by the standing-wave field of the probe laser, whose frequency is resonant to $6^2S_{1/2}|F{=}4{>}\rightarrow 6^2P_{3/2}|F'{=}5{>}$, and the scattered fluorescence is collected by a high-speed PIN photodiode (PD) with large receiving area (10×10 mm^2). The photocurrent output of the PD is amplified by a high-gain trans-impedance amplifier, whose voltage output is recorded by a data acquisition (DAQ) card. The recorded time of flight (TOF) signal is used to diagnose the operation status of the fountain clock.

A typical set of the TOF signals involving both the launching and the returning atomic clouds (not recorded in same fountain cycle) are shown in Fig. 3. The launching atomic

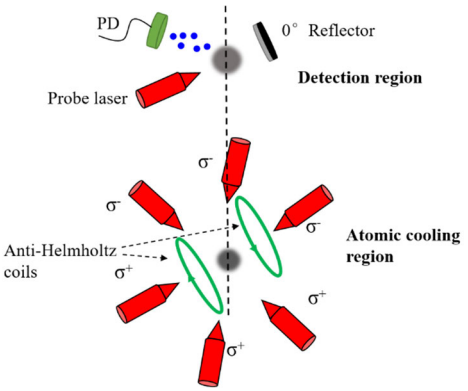

FIGURE 2. Schematic diagram of the laser cooling and trapping in the atomic cooling region, and the TOF signal acquisition in the detection region.

number N_1 and returning atomic number N_2 are calculated according to Eq. (2), respectively [22].

$$\int V(t)dt = G \cdot N \cdot \gamma_0 \cdot \Omega/(4\pi) \cdot \eta \cdot \Delta t \cdot h\nu, \qquad (2)$$

where $V(t)$ is the recorded voltage of the TOF signal in time domain, G is the gain of the trans-impedance amplifier, N is the detected atomic number, γ_0 is the scattering rate of the probe laser, Ω is the detector solid angle perceived by the atomic cloud, η is the photo responsivity of the PD, Δt is the transit time of the atomic cloud, and $h\nu$ is the single photon energy. Here h is the Planck constant, and ν is the frequency of the emitted fluorescent light. The R-L ratio is measured as N_2/N_1.

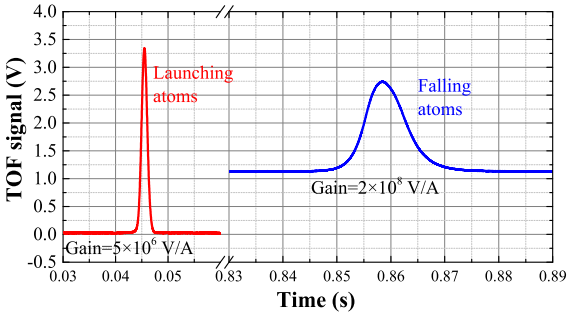

FIGURE 3. Typical TOF signals of the launching and returning atomic clouds in time domain. Different background levels are due to the fact that the current offset and gain in the trans-impedance amplifier are different when the atomic cloud is detected in the launching or returning process. A higher gain is used in the detection of the returning atoms since less atoms are available at that stage.

Theoretically, the relationship between the size of the atomic cloud in the launching direction and the evolution time could be represented as

$$\sigma(t)^2 = \sigma(0)^2 + \tilde{v}^2 \cdot t^2, \qquad (3)$$

where t is the evolution time, $\sigma(t)$ is the root mean square value of the radius of the atomic cloud, $\tilde{v}^2$ is the mean square value of the actual one dimensional velocity for each atom. Thus the atomic temperature T could be calculated by Eq. (4) [22],

$$k_B T = M \cdot \tilde{v}^2, \qquad (4)$$

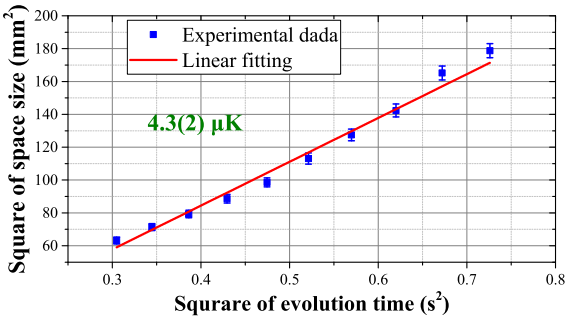

FIGURE 4. Spatial size of the atomic cloud versus the evolution time.

where k_B is the Boltzmann constant, and M is the mass of a single cesium atom.

In the stage of MOM, the cold atomic cloud is launched by producing a relative frequency offset between the six beams of the cooling laser within 2 ms. Since the size of the atomic cloud in the launching direction and the evolution time can be measured when the atomic cloud passes the detection region, the atomic cloud size as a function of the evolution time t can be measured by changing the initial launching speed of the atomic cloud v_0, and the result is shown in Fig. 4. According to Eq. (3), Eq. (4), and the fitting slope $\tilde{v}^2$ given in Fig. 4, the atomic temperature is measured to be 4.3(2) μK. Thus in the Monte Carlo simulation below, the atomic temperature is chosen as 4.3 μK unless specified otherwise.

Structural profile of the integrated microwave cavity is illustrated in Fig. 5(a). Its overall length is 308.1 mm, and the internal diameter of the cut-off waveguide is 12 mm. If the launching direction deviates from the mechanical axis, the R-L ratio will be affected. Several cases that the atomic path deviates from the mechanical axis are given in Fig. 5, where the microwave cavity is simplified as a cylindrical tube. In Fig. 5(b), the atomic path overlaps with the mechanical axis, which is the ideal case. In Fig. 5(c), there is a relative tilt in the atomic path with respect to the mechanical axis. In Fig. 5(d), the atomic path is parallel to the mechanical axis, but there is an offset in the initial launching position. In Fig. 5(e), there are both a relative tilt and an offset in the atomic path with respect to the mechanical axis.

In many cases as shown in Fig. 5, analytic calculation of the R-L ratio is quite complicated. Besides, there may also exist a relative tilt between the mechanical axis and the gravity axis. In the experiment, the mechanical axis is calibrated to be along the gravity axis by reflecting a downward laser beam from a horizontal plane that is defined by a pot of water, and ensure that the reflected beam overlaps with the incident beam. However, limited by the machining and assembly errors, the alignment error of the gravity axis with respect to the mechanical axis is ± 2 mrad. Thus in this paper, the Monte Carlo method is utilized to simulate the whole process, aiming to investigate the factors limiting the R-L ratio quantitatively, and attempt to improve the R-L ratio experimentally via optimization of the relevant parameters.

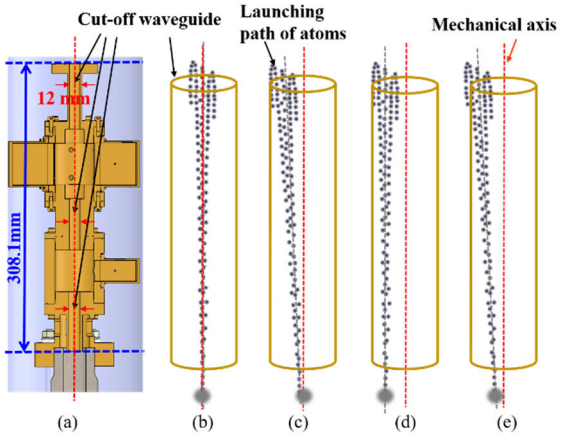

FIGURE 5. (a) Sketch of the integrated microwave cavity. (b), (c), (d), (e) show the representative atomic paths in the integrated microwave cavity.

III. MONTE CARLO SIMULATION MODEL

At the initial moment of atomic launching, the atomic velocity distribution can be written according to the Maxwell-Boltzmann velocity distribution law for dilute cesium gases,

$$f(v_x, v_y, v_z) = \left(\frac{1}{2\pi\tilde{v}^2}\right)^{3/2} \exp\left(-\frac{v_x^2 + v_y^2}{2\tilde{v}^2}\right) \exp\left[-\frac{(v_z - v_0)^2}{2\tilde{v}^2}\right], \tag{5}$$

where v_0 is the initial launching speed of the atomic cloud. In order to describe the evolution of the atomic cloud, one Cartesian coordinate frame (x, y, z) is set up, with z axis along the launching direction of the atomic cloud. Another Cartesian coordinate frame (X, Y, Z) is also configured to describe the physical system, with Z-direction along the mechanical axis. Schematic plot of the two coordinate frames is illustrated in Fig. 6, where the angle between z axis and Z axis is α.

The Monte Carlo simulation is performed as follows. A matrix of $10^6 \times 6$ random numbers is generated in a MATLAB script to simulate the positions and velocities of 10^6 atoms at the initial moment. Six random numbers in each row of the matrix describe the three-dimensional velocity and position components $(v_{ix}, v_{iy}, v_{iz}, x_i, y_i, z_i)$, while random numbers in each column $(i = 1, 2, 3, \ldots, 10^6)$ obey the normal distribution with the mean and root-mean-square values equal to the actual experimental parameters, among which $<v_{ix}> = <v_{iy}> = 0$, $<v_{iz}> = v_0$, $<x_i> = <y_i> = 0$, $<z_i> = -r_0$, $<v_{ix}^2> = <v_{iy}^2> = <(v_{iz} - v_0)^2> = \tilde{v}^2$, $<x_i^2> = <y_i^2> = <(z_i + r_0)^2> = A_0^2$. The simulated three-dimensional velocity distribution of the cold cesium atoms is shown in Fig. 7(a), while the spatial distribution is shown in Fig. 7(b). Both distributions are consistent with the Gaussian distribution.

If the atomic launching direction coincides with the mechanical axis, and the mechanical axis (Z axis) is aligned with the gravity axis, after a free expansion time of t, the position of each single atom is $[x_i(t), y_i(t), z_i(t)] = [x_0 + x_i + v_{ix}t, y_0 + y_i + v_{iy}t, z_0 + z_i - r_0 + (v_{iz+}v_0)t - 1/2gt^2]$, where g is

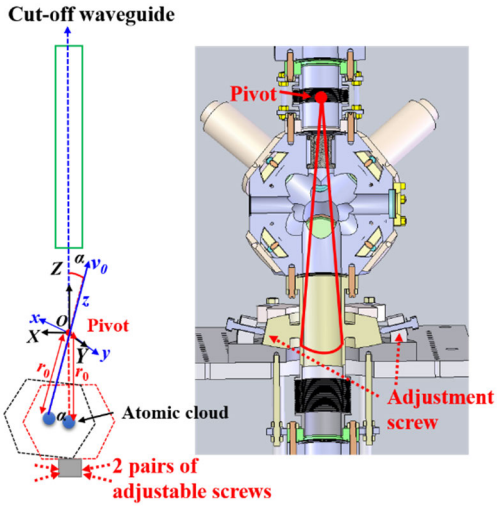

FIGURE 6. Schematic diagram of the direction adjustment mechanism. There is an angle α between the z direction and Z direction. Distance between the pivot and center of the atomic cooling region is r_0. Launching direction of the atomic cloud can be fine tuned with two pairs of adjustable screws. Positive value of α corresponds to clockwise rotation with respect to the coordinate frame (X, Y, Z).

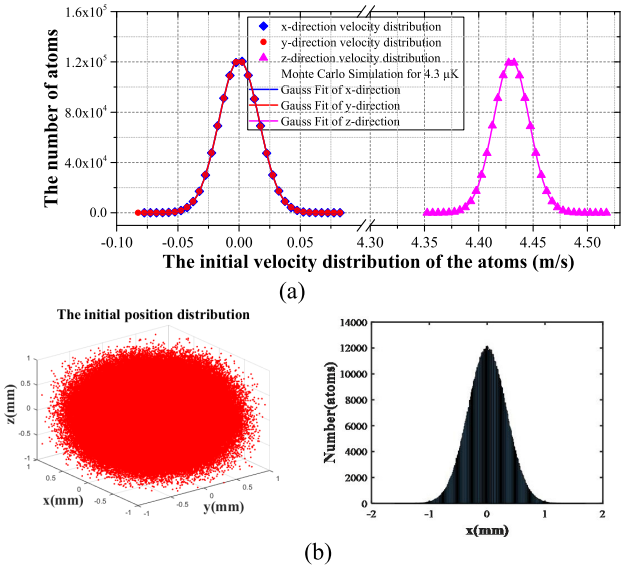

FIGURE 7. (a) The velocity distribution of the atoms in the x, y and z directions. The initial launching speed of the atomic cloud is 4.43 m/s, and the atomic temperature is 4.3 μK. (b) The spatial distribution of the atoms.

the local gravitational acceleration, $[x_0, y_0, z_o]$ is the initial position of the center of the atomic cloud. Since the number of returning atoms is mainly affected by geometric constraint of the cut-off waveguide, it is assumed that the atoms can pass through the cut-off waveguide and reach the detection region as long as $[x_i(t)]^2 + [y_i(t)]^2 \leq R^2$, where R is the inner radius of the cut-off waveguide. The R-L ratio can be calculated by counting the number of cold atoms that can pass the cut-off waveguide, whose value is then divided by the total atomic number used for simulation (1×10^6).

To validate the reliability of the Monte Carlo simulation method, in the beginning we assume z axis, Z axis and the gravity axis all overlap. In such a condition, the R-L ratio can

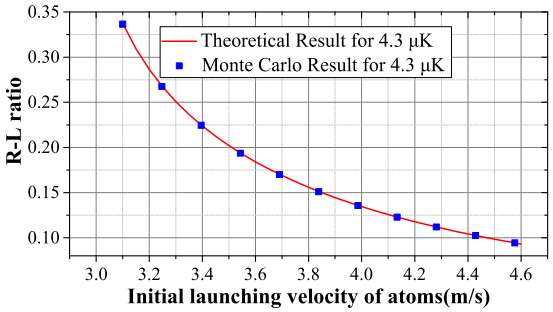

FIGURE 8. Comparison of the R-L ratio between the Monte Carlo simulation results and theoretical results. The initial temperature of the atoms is set as 4.3 μK, and the initial atomic cloud diameter is set as 2 mm.

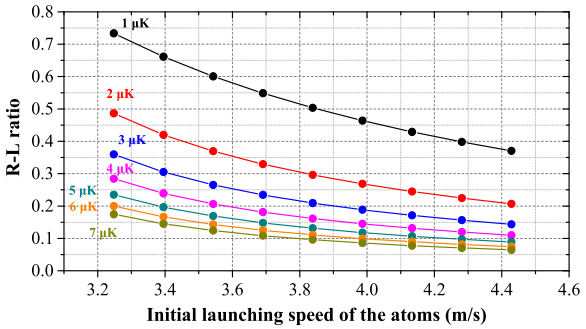

FIGURE 9. Curve of the R-L ratio as a function of initial launching speed. Several curves are plotted for different atomic temperatures.

be calculated with a theoretical formula [23],

$$P_{R-L} = 1 - \exp\left[-R^2/2\sigma^2(t)\right], \tag{6}$$

where R is the inner radius of the cut-off waveguide, and $\sigma(t)$ is the radius of the atomic cloud at time t. Both the theoretical result and the simulation result are given in Fig. 8. As the initial launching speed increases, the spatial size of the atomic cloud becomes larger, and the R-L ratio drops rapidly. It can be seen that the result obtained by the Monte Carlo simulation agrees well with that of the theoretical calculation. However, the theoretical calculation is valid only for the above mentioned ideal condition, while it is difficult to apply to the conditions that there exist angle offsets among the atomic launching direction (z axis), the mechanical axis (Z axis), and the gravity axis, which can be simulated by the Monte Carlo method.

Using Monte Carlo simulation, the factors that limit the R-L ratio are investigated quantitatively, including atomic temperature, tilt angles between z axis and Z axis, and position offsets. To simplify the analysis, the mechanical axis is set parallel to the gravity axis.

A. INFLUENCES OF ATOMIC TEMPERATURE

The atomic cloud with a temperature of several μK is still expanding with the time, and the rate of expansion is determined by the atomic temperature. Thus, it is natural that the spatial size of the atomic cloud when arriving at the microwave cut-off waveguide is affected by the atomic temperature. Using the Monte Carlo simulation method, the relationships between different initial launching speeds and the R-L ratios are given for different atomic temperatures, as shown in Fig. 9. It can be seen that, given a certain number of initial launching atoms, the detected atomic number will benefit a lot with a lower atomic temperature.

B. INFLUENCES OF TILT ANGLES

Compared with the ideal condition that z axis, Z axis and the gravity axis are coincident with each other (see Fig. 5(b)), when there is an angular offset α between z axis and Z axis (see Fig. 5(c)), a portion of atoms may deviate from the vertical path and fall outside the region of the cut-off waveguide, leading to a decrease in the R-L ratio. In this condition, the initial launching speed v_0, can be separated into two velocity components in the coordinate frame (X, Y, Z) defined by the mechanical axis, one along Z-direction $v_1 = v_0\cos\alpha$, while the other is assumed along X-direction $v_2 = v_0\sin\alpha$. Thus, Eq. (5) can be rewritten as

$$f(v_X, v_Y, v_Z) = \left(\frac{1}{2\pi\tilde{v}^2}\right)^{3/2} \exp\left(-\frac{v_X^2}{2\tilde{v}^2}\right) \times \exp\left[-\frac{(v_Y - v_2)^2 + (v_Z - v_1)^2}{2\tilde{v}^2}\right]. \tag{7}$$

Reconstructed three-dimensional velocity and position components of atoms are $[v_{iX}, v_{iY}, v_{iZ}, X_i, Y_i, Z_i]$ in the (X, Y, Z) coordinate frame. The relationship between $[v_{ix}, v_{iy}, v_{iz}, x_i, y_i, z_i]$ and $[v_{iX}, v_{iY}, v_{iZ}, X_i, Y_i, Z_i]$ is established by the rotational matrix, whose expression is given in Eq. (8).

$$\begin{pmatrix} v_{iX} & X_i \\ v_{iY} & Y_i \\ v_{iZ} & Z_i \end{pmatrix} = \begin{pmatrix} \cos\alpha & 0 & \sin\alpha \\ 0 & 1 & 0 \\ -\sin\alpha & 0 & \cos\alpha \end{pmatrix} \begin{pmatrix} v_{ix} & x_i \\ v_{iy} & y_i \\ v_{iz} + v_0 & z_i - r_0 \end{pmatrix}. \tag{8}$$

More complicated case when the other velocity component is not exactly along X-direction can be similarly analyzed. As mentioned previously, the atomic launching direction can be varied by tuning the two pairs of goniometric adjustment screws. We first adjust the screws in the X direction with an angle θ_1, and then adjust the screws in the Y direction with an angle θ_2. Then the angle between the z axis and the Z axis will be α, and the angle between the projection onto the XY plane and the X axis is defined as β, as shown in Figure. 10.

In Fig. 10, the (x, y, z) coordinate frame defined by the atomic launching direction rotate θ_1 about the y axis to (x', y', z'), and then rotate θ_2 about the x' axis to (x'', y'', z''). The point A, point B and point C are the central positions of the atomic cloud. The central positions of the atomic cloud are constantly changing with the 3D-MOT adjustment. According to the rotational matrix with respect to the coordinate transformation, Eq. (8) can be rewritten as

$$R_y(\theta_1) = \begin{pmatrix} \cos\theta_1 & 0 & \sin\theta_1 \\ 0 & 1 & 0 \\ -\sin\theta_1 & 0 & \cos\theta_1 \end{pmatrix},$$

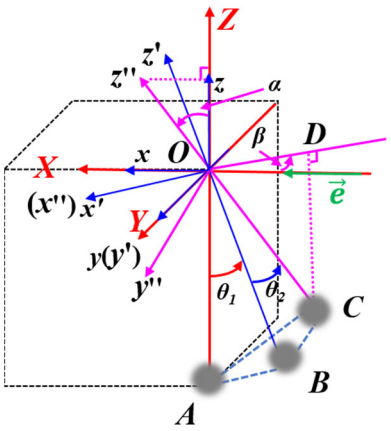

FIGURE 10. Schematic diagram of the goniometric adjustment in the atomic cooling region. Two successive variations in angles are θ_1 and θ_2, respectively. $\overrightarrow{OA} = (0, 0, -r_0)$, and $\vec{e}$ is a unit vector in the X direction. When the angles θ_1 and θ_2 are zero, α and β are also zero.

$$R_{x'}(\theta_2) = \begin{pmatrix} 1 & 0 & 0 \\ 0 & \cos\theta_2 & \sin\theta_2 \\ 0 & -\sin\theta_2 & \cos\theta_2 \end{pmatrix},$$

$$\begin{pmatrix} v_{iX} & X_i \\ v_{iY} & Y_i \\ v_{iZ} & Z_i \end{pmatrix} = R_{x'}(\theta_2) R_y(\theta_1) \begin{pmatrix} v_{ix} & x_i \\ v_{iy} & y_i \\ v_{iz} + v_0 & z_i - r_0 \end{pmatrix}. \quad (9)$$

The relationship between angles θ_1, θ_2 and angles α, β is given in Eq. (10) and Eq. (11),

$$\cos\alpha = \frac{\overrightarrow{AO} \cdot \overrightarrow{CO}}{\left|\overrightarrow{AO}\right| \left|\overrightarrow{CO}\right|} = \cos\theta_1 \cos\theta_2, \quad (10)$$

$$\cos\beta = \frac{\overrightarrow{DO} \cdot \overrightarrow{e}}{\left|\overrightarrow{DO}\right| \left|\overrightarrow{e}\right|} = \frac{\sin\theta_1}{\sqrt{\sin^2\theta_1 + \sin^2\theta_2 \cos^2\theta_1}}. \quad (11)$$

Thus, the relationship between the R-L ratio and the two sets of angles, including θ_1, θ_2 and α, β, is illustrated in Fig. 11. It can be seen from Fig. 11(a) that the R-L ratio peaks when both θ_1 and θ_2 approach zero, and decreases with the increase in either θ_1 or θ_2. On the other hand, the R-L ratio is heavily dependent on α, but is insensitive to variation of β, as shown in Fig. 11(b).

C. INFLUENCES OF OFFSET (x_0, y_0, z_0)

Due to spatial inhomogeneity in magnetic environment and asymmetry between various beams of the cooling laser, at the initial moment, there might exist a position offset between the atomic cloud and the geometric center of the atomic cooling region (see Fig. 5(d)), while the launching direction (z axis) is parallel to the mechanical axis (Z axis). Here the position offset is set as (x_0, y_0, z_0). Thus, compared with the ideal condition, a portion of atoms is easier to fall beyond the cut-off waveguide, leading to a decrease in the R-L ratio.

A displacement vector is used to transform the description of the three-dimensional velocity and position of the atoms from (x, y, z) coordinate frame to (X, Y, Z) coordinate frame. The corresponding transformation between

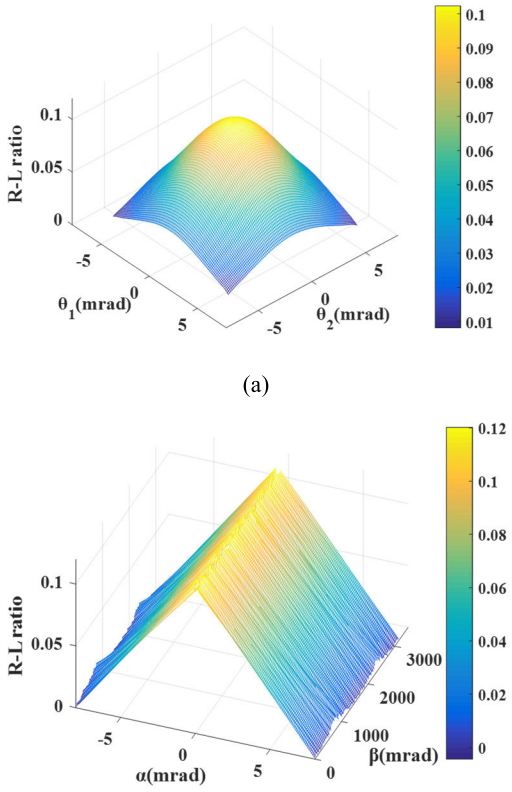

FIGURE 11. (a) The variation in R-L ratio with angles θ_1 and θ_2. (b) The variation in R-L ratio with angles α and β.

(v_{ix}, v_{iy}, v_{iz}, x_i, y_i, z_i) and (v_{iX}, v_{iY}, v_{iZ}, X_i, Y_i, Z_i) is given in Eq. (12),

$$\begin{pmatrix} v_{iX} & X_i \\ v_{iY} & Y_i \\ v_{iZ} & Z_i \end{pmatrix} = \begin{pmatrix} v_{ix} & x_i \\ v_{iy} & y_i \\ v_{iz} & z_i - r_0 \end{pmatrix} + \begin{pmatrix} 0 & x_0 \\ 0 & y_0 \\ v_0 & z_0 \end{pmatrix}. \quad (12)$$

The beam diameter of the cooling lasers used to trap the cold atoms is 20 mm. Considering the limited trap region of the light field, the offsets used in the simulation process shall not be too large. Several sets of position offsets are selected to analyze the influence on the R-L ratio, whose simulation results are shown in Fig. 12(a). It can be seen that, when the initial launching speed is small, the position offset value has a significant influence on the R-L ratio, while the influence becomes negligible when the speed exceeds 4 m/s. Since the initial launching speed is 4.43 m/s in the actual atomic fountain experiment, a position offset of 0-4 mm will have a small influence on the R-L ratio. In addition, since the velocity distribution of the atomic cloud is isotropic in the X, Y plane, given a constant $<Z_i>$, the curve of the R-L ratio is identical as long as the $<X_i>^2 + <Y_i>^2$ value is the same, as shown in Fig. 12(b).

D. INFLUENCES OF ANGLES α, β AND OFFSET (x_0, y_0, z_0)

We now consider the case that the R-L ratio is influenced by both the angle offset α, β and the position offset (x_0, y_0, z_0) in the (X, Y, Z) coordinate frame (see Fig. 5(e)). In this

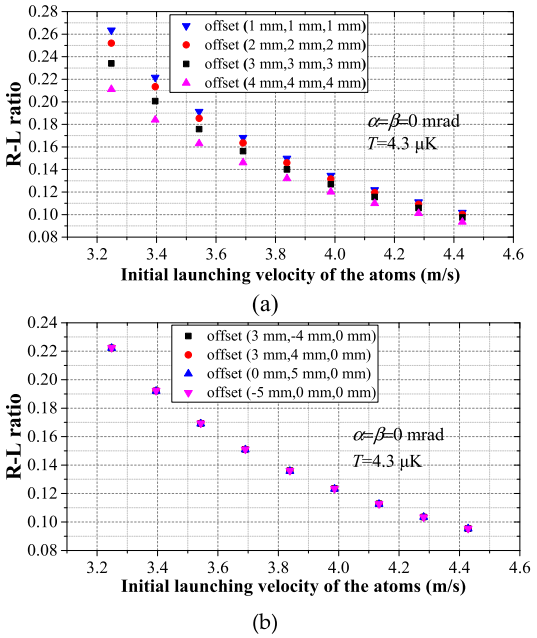

FIGURE 12. Curve of the R-L ratio as a function of the initial launching speed, and several sets of position offsets are given to analyze the influence of different position offsets on the R-L ratio. The position unit is in mm. (a) Position offsets are set as (1, 1, 1), (2, 2, 2), (3, 3, 3) and (4, 4, 4), respectively. (b) Position offsets are set as (3, −4, 0), (3, 4, 0), (0, 5, 0) and (−5, 0, 0), respectively.

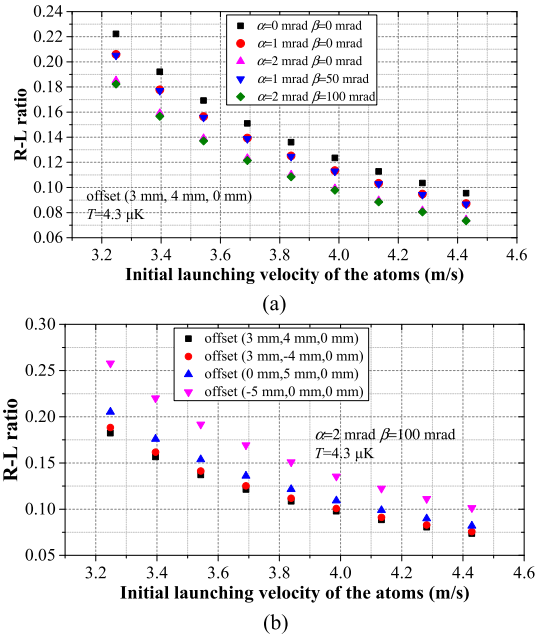

FIGURE 13. Curve of the R-L ratio as a function of the initial launching speed, and sets of position offsets or angle offsets are given to analyze the influence on the R-L ratio. The position unit is in mm. (a) Angle offsets (α, β) are set as (0 mrad, 0 mrad), (1 mrad, 0 mrad), (2 mrad, 0 mrad), (1 mrad, 50 mrad), and (2 mrad, 100 mrad), respectively, while the position offset is set to a fixed value (3, 4, 0). (b) The position offsets are set as (3, 4, 0), (3, −4, 0), (0, 5, 0), and (−5, 0, 0), respectively. Angle offset (α, β) is (2 mrad, 100 mrad).

condition, the transformation between $(v_{ix}, v_{iy}, v_{iz}, x_i, y_i, z_i)$ and $(v_{iX}, v_{iY}, v_{iZ}, X_i, Y_i, Z_i)$ is

$$\begin{pmatrix} v_{iX} & X_i \\ v_{iY} & Y_i \\ v_{iZ} & Z_i \end{pmatrix} = R_{x'}(\theta_2) R_y(\theta_1) \begin{pmatrix} v_{ix} & x_i + x_0 \\ v_{iy} & y_i + y_0 \\ v_{iz} + v_0 & z_i - r_0 + z_0 \end{pmatrix}. \tag{13}$$

Given a certain position offset, several sets of angle offsets are selected to analyze the influence on the R-L ratio, whose simulation result is shown in Fig. 13(a). Similar to the conclusion given in Fig.11, the R-L ratio is still heavily dependent on α, while it is insensitive to the variation in β. In addition, given a certain set of angle offsets α and β, a set of position offsets is also selected to analyze the influence on the R-L ratio, and the result is shown in Fig. 13(b). Compared with the simulation result given in Fig. 12(b), the curves of the R-L ratio as a function of the initial atomic launching speed diverge from each other in the presence of different position offsets, although the $<X_i>^2 + <Y_i>^2$ value is the same.

Thus, according to the Monte Carlo simulation, the physical variables, including the angle offset and the position offset, together with the atomic temperature, all have an effect on the R-L ratio, and the quantitative dependence relationship between the R-L ratio and these factors is calculated here.

E. SIMULATION OF RAMSEY FRINGE

In the development of an atomic fountain clock, acquisition of Ramsey fringe is one of the landmark achievements, which lays the foundation for clock frequency servo locking. For a single atom with a typical velocity v, the transition probability after Ramsey interaction is represented as

$$P(v) = 4\left(\frac{\Omega}{\Omega'}\right)^2 \sin^2\frac{\Omega'\tau(v)}{2}\left[\cos\frac{\Omega'\tau(v)}{2}\cos\frac{\Delta T(v)}{2} - \frac{\Delta}{\Omega'}\sin\frac{\Omega'\tau(v)}{2}\sin\frac{\Delta T(v)}{2}\right]^2. \tag{14}$$

Here Ω_0 is the Rabi frequency, Δ is the microwave frequency detuning, $\Omega' = (\Delta^2 + \Omega_0^2)^{1/2}$ is the generalized Rabi frequency, $\tau(v)$ is the atom-microwave interaction time for single microwave pulse in the Ramsey cavity, and $T(v)$ is the free evolution time of the atom. We use Monte Carlo method to generate a set of random numbers, with individual random number representing the velocity of an atom in the z axis, $<v_{iz}> = v_1$, $<(v_{iz} - v_1)^2> = \tilde{v}^2$. Here v_1 is the mean velocity of the atomic cloud when arriving at the Ramsey cavity. The simulated Ramsey fringe is the summation of the Ramsey fringe for each atom, divided by the atomic number. The result for atomic clouds with the atomic temperatures of 6 μK and 2 μK is shown in Fig. 14. Although the atomic temperature does not affect the contrast of the central Ramsey fringe directly, the bottom hollow part of the Ramsey fringe is smaller at a lower atomic temperature.

IV. EXPERIMENTAL RESULTS

Experiments are performed on our developed cesium atomic fountain clock to verify the Monte Carlo simulation result on the R-L ratio, and the R-L ratio and Ramsey fringe contrast are optimized. Power in the six beams of the cooling laser is balanced, and the earth magnetic field is compensated

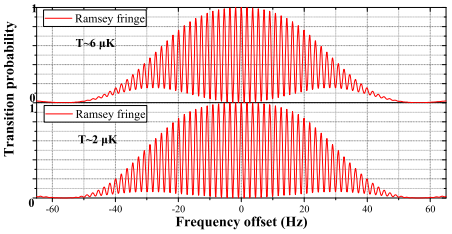

FIGURE 14. The Ramsey fringe simulated with Monte Carlo method. The atomic temperatures of the atomic clouds are 6 μK and 2 μK, respectively.

using three sets of Helmholtz coils. In the MOT stage, optical intensities of the repumping laser and each cooling laser beam are 0.4 mW/cm^2 and 2.5 mW/cm^2, respectively, and the maximum magnetic field gradient is ∼5.6 Gauss/cm. In the OM stage, the optical intensity of the cooling laser beam is lowered to half of the original, while the magnetic field gradient drops to zero. In the MOM stage, the optical intensity of the cooling laser is further dropped to zero in 1 ms, and the repumping laser shuts down before a time delay of 5 ms. In the detection stage, the optical intensity of the detection laser is ∼2.5 mW/cm^2, and the gain of the trans-impedance amplifier for the ascent and descent TOF signal detection are 5×10^6 V/A and 2×10^8 V/A, respectively. The goniometric adjustment unit is used to tune the angles θ_1, θ_2, whose values are measured simultaneously by a two-dimensional tilt meter (Model: Jewell 755), aiming to optimize the R-L ratio.

The simulation and measurement curve of the R-L ratio as a function of angle α is shown in Fig. 15. At an angle offset α of -2.5 mrad, the measurement result approaches the peak, and the value is 8.6%±0.4%. However, according to the simulation results in Fig. 11, the peak should be obtained when the angle α is zero. This is due to the fact that the angle offset between the mechanical axis and the gravity axis cannot be adjusted to zero due to adjustment resolution of 2 mrad. To take this into account, a Monte Carlo simulation is made for the case that there exists an angle offset $\gamma = 2$ mrad between the mechanical axis and the gravity axis, whose result is also shown in Fig. 15, and a better fit for the simulation result and the experimental result is obtained. At an angle offset α of -2.5 mrad, the simulation peak is about 9.6%. Although both curves follow the same tendency that the R-L ratio peaks, the measurement value is not as large as the simulation one. The result may be explained as follows. The number of atoms launched into the fluorescence detection zone is N_0, the number of atoms returning back to the fluorescence detection zone is N_1, the ratio of the returning atoms is $\eta_0 = N_1/N_0$. We lost $\xi_0 N_0$ atoms in the flight due to collisions with residual gases in free evolution [24], or there is a part of cold atoms with higher temperature in the launching atomic cloud. The calculation error of the number of atoms introduced by the difference in detection efficiency of fluorescence detector is $\xi_1 N_1$. Taking these into account, the R-L ratio is modified as $\eta = (1 - \xi_1)\,\eta_0 + \xi_0$, and $\xi_1 = 0.07$, $\xi_0 = 0.02$. Fig. 15 shows that the variation trend of experimental values with modification is now consistent with that of the simulation values.

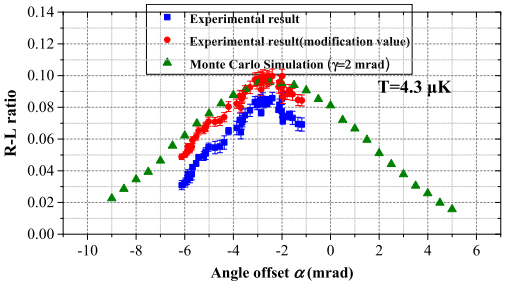

FIGURE 15. Comparison between simulation and measurement result of the R-L ratio as a function of angle α. A Monte Carlo simulation for an angle offset $\gamma = 2$ mrad between the mechanical axis and the gravity axis is assumed.

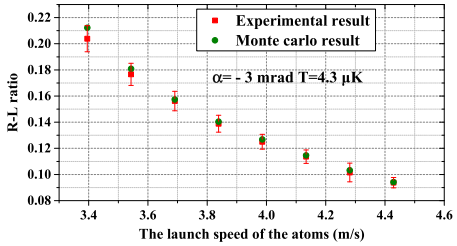

FIGURE 16. Comparison between the simulation and the measurement curve of the R-L ratio as a function of the initial launching speed of the atoms. The angle offset γ between the mechanical axis and the gravity axis is set as 2 mrad.

In the stage of MOM, the initial launching speed of the atomic cloud can be changed by varying the relative frequency offset between the six beams of the cooling laser. Thus, after optimization of the angle offset, a curve of the R-L ratio as a function of the initial launching speed can be measured, whose result is shown in Fig. 16. Meanwhile, a Monte Carlo simulation result is also given for the case that there exists an angle offset $\gamma = 2$ mrad between the mechanical axis and the gravity axis. The modified experimental results and the simulation result show that the R-L ratio drops with the increase in the initial launching speed have the same tendency.

After the R-L ratio is optimized, the atoms in $|F = 3, m_F = 0>$ state is selected with the microwave field oscillating in the selection cavity and a downward push laser. For ^{133}Cs atoms, eight-ninths of the atoms will be lost after state selection theoretically. Then the atoms experience two $\pi/2$ microwave interaction when they pass twice through the Ramsey cavity in the ascent and descent trajectory, and project the microwave frequency detuning message to the transition probability of the atoms, which is then detected in the detection region. The Ramsey fringe is obtained by scanning the microwave frequency detuning.

The contrast of the Ramsey fringe is limited by the purity of the quantization axis (C-field) [25]. In the atomic fountain experiment, the C-field is generated by a long solenoid, which is driven by a high precision current source. By increasing the current slightly, the contribution of the stray magnetic field is suppressed, and the contrast of the Ramsey fringe increases from less than 70% to 90%, as shown in Fig. 17.

Following the simulation guidance that the pattern of Ramsey fringe is affected by the atomic temperature, the atomic

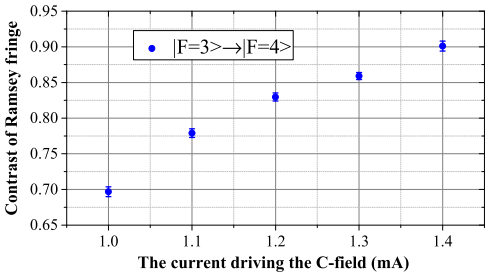

FIGURE 17. Measurement contrast of the central Ramsey fringe versus the current driving the C-field.

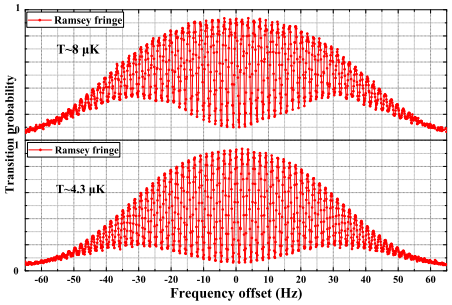

FIGURE 18. Measured Ramsey fringe pattern for the cesium atomic fountain clock with the atomic temperatures of 8 μK and 4.3 μK, respectively.

temperature is changed between 8 μK and 4.3 μK, and the measured Ramsey fringe are shown in Fig. 18. The measurement result verifies the simulation conclusion that the bottom hollow part of the Ramsey fringe is smaller at a lower atomic temperature. It can also be seen that the contrast of the central Ramsey fringe for an atomic temperature of 4.3 μK is about 90%, which can be further improved by minimizing the microwave leakage, optimizing the detection efficiency, purifying the C-field. Acquisition of a high-quality Ramsey fringe lays the foundation for the clock frequency servo locking in the future.

V. CONCLUSION

Given the convenience of the Monte Carlo method in tracing the atomic path in an atomic fountain, we use it to simulate the relationship between the R-L ratio and physical variables, including the atomic temperature, launching direction of the atomic cloud, and the initial position of the atomic cloud. According to the reasonable range of the physical variables, the quantitative relationship with the R-L ratio is given, which provides a guideline for experimental optimization of the R-L ratio. A cesium atomic fountain experiment has been performed, and an R-L ratio of 8.6%±0.4% is ultimately obtained for a cesium atomic fountain with a launching height of ∼1 m, which approaches the simulation result of 9.6% for an atomic temperature of 4.3 μK.

The Monte Carlo method is also used to simulate the Ramsey fringe, and it is found that the pattern of the Ramsey fringe is affected by the atomic temperature, which is also verified in the actual experiment. In addition, the contrast of the central Ramsey fringe is experimentally optimized to 90%, which lays a good foundation for the servo locking of the cesium atomic fountain clock in the future. The Monte Carlo simulation we use can also be applied to evaluate various systematic uncertainties of atomic fountain clocks, such as distributed cavity shift, collision shift, Doppler shift, etc. The simulation result will be reported in another publication when our fountain clock finish full systematic uncertainty evaluation.

The R-L ratio in the cesium atomic fountain clock is still not extremely high, which remains a limitation on the increase of the detected atomic number. In the future, we will continue to improve the R-L ratio by lowering the atomic temperature, aiming to improve the atomic number ultimately. We will also improve the contrast of Ramsey fringe using various techniques.

REFERENCES

[1] G. D. Rovera, S. Bize, B. Chupin, J. Guéna, P. Laurent, P. Rosenbusch, P. Uhrich, and M. Abgrall, "UTC(OP) based on LNE-SYRTE atomic fountain primary frequency standards," *Metrologia*, vol. 53, no. 3, pp. S81–S88, Jun. 2016.

[2] X. Wang, F. Shi, D. Gong, S. Xu, Z. Li, G. Fu, and Q. Li, "Realization of a free-running timescale based on a CsF1 cesium fountain clock and multiple active hydrogen masers," *Metrologia*, vol. 57, no. 6, Dec. 2020, Art. no. 065009.

[3] N. Ashby, T. E. Parker, and B. R. Patla, "A null test of general relativity based on a long-term comparison of atomic transition frequencies," *Nature Phys.*, vol. 14, no. 8, pp. 822–826, Aug. 2018.

[4] C. G. Parthey, A. Matveev, J. Alnis, B. Bernhardt, A. Beyer, R. Holzwarth, A. Maistrou, R. Pohl, K. Predehl, T. Udem, T. Wilken, N. Kolachevsky, M. Abgrall, D. Rovera, C. Salomon, P. Laurent, and T. W. Hänsch, "Improved measurement of the hydrogen 1S–2S transition frequency," *Phys. Rev. Lett.*, vol. 107, no. 20, Nov. 2011, Art. no. 203001.

[5] Q. Wang, A. Matveev, J. Alnis, B. Bernhardt, A. Beyer, R. Holzwarth, A. Maistrou, R. Pohl, K. Predehl, T. Udem, T. Wilken, N. Kolachevsky, M. Abgrall, D. Rovera, C. Salomon, P. Laurent, and T. W. Hänsch, "Precision measurements of the ground-state hyperfine splitting of Rb 85 using an atomic fountain clock," *Phys. Rev. A, Gen. Phys.*, vol. 100, no. 2, Aug. 2019, Art. no. 022510.

[6] S. Peil, T. B. Swanson, J. Hanssen, and J. Taylor, "Microwave-clock timescale with instability on order of 10–17," *Metrologia*, vol. 54, no. 3, pp. 247–252, Jun. 2017.

[7] A. Bauch, "Caesium atomic clocks: Function, performance and applications," *Meas. Sci. Technol.*, vol. 14, no. 8, p. 1159, 2003.

[8] (2019). *BIPM Annual Report on Time Activities*. [Online]. Available: https://www.bipm.org/en/time-ftp/annual-reports

[9] F. Levi, D. Calonico, C. E. Calosso, A. Godone, S. Micalizio, and G. A. Costanzo, "Accuracy evaluation of ITCsF2: A nitrogen cooled caesium fountain," *Metrologia*, vol. 51, no. 3, pp. 270–284, Jun. 2014.

[10] T. P. Heavner, S. R. Jefferts, E. A. Donley, J. H. Shirley, and T. E. Parker, "NIST-F1: Recent improvements and accuracy evaluations," *Metrologia*, vol. 42, no. 5, pp. 411–422, Oct. 2005.

[11] J. Guéna, M. Abgrall, D. Rovera, P. Laurent, B. Chupin, M. Lours, G. Santarelli, P. Rosenbusch, M. E. Tobar, R. Li, K. Gibble, A. Clairon, and S. Bize, "Progress in atomic fountains at LNE-SYRTE," *IEEE Trans. Ultrason., Ferroelectr., Freq. Control*, vol. 59, no. 3, pp. 391–409, Mar. 2012.

[12] T. P. Heavner, E. A. Donley, F. Levi, G. Costanzo, T. E. Parker, J. H. Shirley, N. Ashby, S. Barlow, and S. R. Jefferts, "First accuracy evaluation of NIST-F2," *Metrologia*, vol. 51, no. 3, pp. 174–182, Jun. 2014.

[13] G. Santarelli, P. Laurent, P. Lemonde, A. Clairon, A. G. Mann, S. Chang, A. N. Luiten, and C. Salomon, "Quantum projection noise in an atomic fountain: A high stability cesium frequency standard," *Phys. Rev. Lett.*, vol. 82, no. 23, pp. 4619–4622, Jun. 1999.

[14] F. Riehle, *Frequency Standards: Basics and Applications*. Weinheim, Germany: Wiley, 2006.

[15] F. P. Dos Santos, H. Marion, S. Bize, Y. Sortais, A. Clairon, and C. Salomon, "Controlling the cold collision shift in high precision atomic interferometry," *Phys. Rev. Lett.*, vol. 89, no. 23, Nov. 2002, Art. no. 233004.

[16] J. Guéna, R. Li, K. Gibble, S. Bize, and A. Clairon, "Evaluation of Doppler shifts to improve the accuracy of primary atomic fountain clocks," *Phys. Rev. Lett.*, vol. 106, no. 13, Apr. 2011, Art. no. 130801.
[17] S. Beattie, B. Jian, J. Alcock, M. Gertsvolf, R. Hendricks, K. Szymaniec, and K. Gibble, "First accuracy evaluation of the NRC-FCs2 primary frequency standard," *Metrologia*, vol. 57, no. 3, Jun. 2020, Art. no. 035010.
[18] K. Szymaniec, W. Chałupczak, E. Tiesinga, C. J. Williams, S. Weyers, and R. Wynands, "Cancellation of the collisional frequency shift in caesium fountain clocks," *Phys. Rev. Lett.*, vol. 98, no. 15, Apr. 2007, Art. no. 153002.
[19] C. Xu, R. Xu, W. Zeng, and J. Yan, "A new high-precision gravity solid tidal model for precision gravity measurement facility," *Geodesy Geodyn.*, vol. 11, p. 265, Jul. 2020.
[20] V. Gerginov, N. Nemitz, S. Weyers, R. Schröder, D. Griebsch, and R. Wynands, "Uncertainty evaluation of the caesium fountain clock PTB-CSF2," *Metrologia*, vol. 47, no. 1, pp. 65–79, 2010.
[21] S. Bize, P. Laurent, M. Abgrall, H. Marion, I. Maksimovic, L. Cacciapuoti, J. Grünert, C. Vian, F. P. dos Santos, P. Rosenbusch, P. Lemonde, G. Santarelli, P. Wolf, A. Clairon, A. Luiten, M. Tobar, and C. Salomon, "Advances in atomic fountains," *Comptes Rendus Physique*, vol. 5, no. 8, pp. 829–843, Oct. 2004.
[22] H. J. Metcalf and P. Van der Straten, *Laser Cooling and Trapping of Neutral Atoms*. Hoboken, NJ, USA: Wiley, 2007.
[23] S. Ghezali, P. Laurent, S. N. Lea, and A. Clairon, "An experimental study of the spin-exchange frequency shift in a laser-cooled cesium fountain frequency standard," *Europhys. Lett.*, vol. 36, no. 1, pp. 25–30, Oct. 1996.
[24] K. Gibble, "Scattering of cold-atom coherences by hot atoms: Frequency shifts from background-gas collisions," *Phys. Rev. Lett.*, vol. 110, no. 18, May 2013, Art. no. 180802.
[25] V. Gerginov, N. Nemitz, and S. Weyers, "Initial atomic coherences and Ramsey frequency pulling in fountain clocks," *Phys. Rev. A, Gen. Phys.*, vol. 90, no. 3, Sep. 2014, Art. no. 033829.

HUI LI was born in Shangqiu, Henan, China, in 1990. She received the B.S. degree from Henan University, China, in 2015. She is currently pursuing the Ph.D. degree with Huazhong University of Science and Technology, China. She is mainly engaged in the development of cesium fountain clock.

YUANBO DU received the B.S. degree from Lanzhou University, China, in 2010, and the Ph.D. degree from the University of Chinese Academy of Sciences, in 2015. Then, he was a Postdoctoral Fellow with Huazhong University of Science and Technology, China. In 2021, he joined the School of Physics and Astronomy, Sun Yat-sen University, China. He is currently an Associate Professor. His research interests include atomic frequency standards, experiments in cold atomic physics, and photonic microwave generation.

XIAN YANG received the B.S. and M.S. degrees from Huazhong University of Science and Technology, China, in 2018 and 2021, respectively. His research interest includes the development of ultra-low phase noise microwave sources based on optical frequency down conversion for cesium fountain clock.

YUNYI GUO received the B.S. degree from Sichuan University, China, in 2019. She is currently pursuing the master's degree with Huazhong University of Science and Technology, China. She is mainly engaged in the development of cesium fountain clock.

MINGMING LIU received the B.S. degree from Ludong University, China, in 2020. She is currently pursuing the master's degree with Huazhong University of Science and Technology, China. She is mainly engaged in the development of cesium fountain clock.

WENBING LI received the Ph.D. degree in radio physics from Wuhan Institute of Physics and Mathematics, Chinese Academy of Sciences, Wuhan, China, in 2016. From 2016 to 2018, he was a Postdoctoral Researcher with Huazhong University of Science and Technology, Wuhan. Since 2018, he has been a Postdoctoral Researcher with Helmholtz-Institut Mainz, Mainz, Germany. His research interests include atomic frequency standard, ultralow noise microwave generation, and high precision optical spectroscopy measurement.

HONGLI LIU received the B.S. degree from China Jiliang University, China, in 2008, and the Ph.D. degree from the University of Chinese Academy of Sciences, China, in 2013. From July 2013 to March 2017, he worked with Nanjing Institute of Advanced Laser Technology. From March 2017 to December 2019, he conducted Postdoctoral Research at Huazhong University of Science and Technology. In 2020, he was a Postdoctoral Fellow at PTB, Braunschweig, Germany. In 2021, he joined the School of Physics, Huazhong University of Science and Technology. His research interests include atomic clock, optical clock, and cold atomic physics.

ZEHUANG LU was born in January 1971. He received the B.S. degree from Xiamen University, China, in 1991, the M.S. degree from Ohio University, USA, in 1994, and the Ph.D. degree from Duke University, USA, in 1999. From 1999 to 2003, he was a Postdoctoral Fellow with the University of Illinois at Urbana–Champaign, USA. From 2004 to 2010, he was the Research Group Leader at Max-Planck Institute for the Science of Light, Germany. He was appointed as a Professor with Huazhong University of Science and Technology, in 2010. His research interests include precision measurement physics, optical frequency standards, and precision laser spectroscopy.